Design, Implementation and Validation of the Large Item Neutron Assay System (LINAS) at the Paducah Gaseous Diffusion Plant (PGDP) – 24043

Marcel Villani[1], Dave Petroka[1], Brian Young[2], Andrew Crabtree[3], Kirill Pushkin[1], Sean Stanfield[1], Scott Price[1], William Mussman[1], Patricia McClay[1], Sasha Philips[1], David Sullivan[1], Matthew McAlear[1], Steven Tommell[1], Brent Montgomery[4], Brian Eells[4], Joseph Hamm[4], Tyler Coriell[4], Taft Adams[4], David Ackley[4] and Bob McElroy[5]

[1]Mirion Technologies (Canberra)
[2]ISO-PACIFIC Remediation Technologies
[3]Matrix Engineering, PLLC
[4]Four Rivers Nuclear Partnership (FRNP)
[5]Oak Ridge National Lab

ABSTRACT

The LINAS is a large, shielded, neutron detection system used for quantifying the holdup mass including passivation layers and deposits of Uranyl Fluoride (UO2F2) located within plant equipment by passive neutron counting. The UO2F2 arises from hydrolyzed uranium hexafluoride (UF6) where the enrichment and mass fractions are well known for the process plant equipment for a given cascade at the Paducah Gaseous Diffusion Plant (PGDP). The plant equipment designated for holdup characterization includes '000' and '00' converters, pipes, valves, compressors, coolers, waste box containers, and smaller components. The plant equipment size ranges from less than two feet to 13.5' in diameter and from a few feet to a maximum of 24' in length. Central to the LINAS infrastructure is a very large concrete shielded chamber with an array of neutron detectors. The chamber is optimally shielded from cosmic ray induced neutron spallation through the material properties of thick concrete and the use of High Density Borated Polyethylene (HDBPE) sheets. Inside the LINAS chamber are High Density Polyethylene (HDPE) clad He-3 pressurized gas detectors, in a cylindrical ring arrangement, which detect the neutrons emitted from the UO2F2 holdup . The plant equipment is placed on heavy duty carts, supported by cradles, and moved through the LINAS chamber stopping at the chamber center position. The thick HDPE sliding doors are closed, and the plant equipment is assayed to determine the total mass of U-235 providing an assessment of the holdup within the plant equipment. Next to the LINAS chamber is the control room where the Data Acquisition System (DAS) electronics are located and connected to the neutron detectors within the LINAS chamber. The objective of this paper is to discuss the design goals based on the Data Quality Objectives (DQO's), implementation of the design and a recent Validation and Verification (V&V) plan, with results, using Working Reference Materials (WRM's) and appropriate surrogate objects representing the plant equipment.

INTRODUCTION

The gaseous diffusion process involves the enrichment of Uranium mostly for the purpose of commercial fuel (3-5%) by forcing high-temperature, low-pressure, UF6 gas through a molecular diffusion barrier where a higher proportion of U-234 and U-235 enters through the barrier than U-238 thus enriching the fissile content [1]. The gaseous diffusion process requires extremely large structural carbon steel (CSTEEL) components of plant equipment involving converters, coolers, compressors, pipes and valves, arranged in a cell, as shown in Fig. 1. Each cell increases the enrichment by an extremely small amount; to attain the final, desired, enrichment, scores of cells are required.

When gas-phase UF6 is exposed to humid air, the UF6 undergoes hydrolysis forming UO2F2 deposits [2]. The source of humid air intrusion involves accidental introduction into the stream via leaks in pipe valves, flanges, expansion joints, connections and welds within the plant equipment. The leaks are due to the lower pressure UF6 gas stream which is purposely less than one atm. The largest of the UO2F2 deposits can be localized and removed *in situ* but the smaller deposits are more difficult to find and remove.

In addition, when UF6 was introduced into the process , significant and permanent, passivation layers immediately begin to accumulate [3].

The Paducah Gaseous Diffusion Plant (PGDP) in Western KY, under deactivation since 2013, utilized several buildings for various enrichment ranges (cascades) where the lowest enrichment (up to 2%) involved '000' (triple-naught) size converters and higher enrichments (>2% but less than 5%) involved '00' (double-naught) size converters. Both the '000' and '00' converters are many feet in length and diameter and weigh several thousand lbs. Under the deactivation and demolition plan, the plant equipment is removed from the cells within each building. For some plant equipment, further disassembly might be required for disposition purposes. For example, the large '000' converters are disassembled to the constituent components which include the large molecular diffusion barrier and cooler. The recycle coolers,'00' converters, '000' and '00' compressors, gate valves and pipes may be extracted as discrete plant equipment. Prior to disposition, the extracted plant equipment must be characterized for fissile (U-235) content where the process knowledge only consists of the gross weight of the large metallic object (plant equipment), and the cascade information which includes the enrichment and the U-235:U-234 weight percent ratio.

The principle waste characterization technique involves detecting and counting neutrons primarily from the prolific U-234 alpha decay interacting with the F-19 nucleus, *i.e.*, F-19 (α,n) Na-22. The alpha decay of U-235 and U-238 also contribute but the reaction cross-sections are orders of magnitude smaller than that of U-234. There are also fewer neutrons generated from UO2F2 involving (α,n) interactions with O-17 as well as neutrons generated from spontaneous fission, especially that of U-238. The neutron detection signal is calibrated as a function of fissile (U-235) mass in grams. The neutron Specific Activity (nSA) for (α,n) reactions with Fluorine and Oxygen [4], [5] are shown in the first two columns of Table 1 for the Uranium isotopes of consideration where the percent Relative Standard Deviation (%RSD) is ± 3%. The third column shows the nSA for Spontaneous Fission (SF) for the same isotopes where U-238 is the largest SF nSA contributor and the %RSD for U-238 is ± 1.7%. Most of the neutron production is from the (α,n) reaction but the contribution from SF is not negligible especially for low enrichments such as is the case at PGDP. The combined nSA for the extremes of hydrolyzation [5] is observed in the first two columns of Table 2 where "wet" corresponds to a hydration level of 4 [2] and "dry" a hydration level of zero. The third column in Table 2 shows the nSA for solid UF6. The range of the hydration level for the holdup corresponds to an uncertainty in the neutron emission if the hydration level is not known for the sample. The extracted plant equipment has been exposed to the environment so the expected hydration level is as high as 4, thus the "wet" nSA is assumed. Sealed WRM's are thoroughly dried when being processed in the analytical lab so WRM's are considered as "dry" nSA.

Table 1 Neutron Specific Activity (nSA) for Fluorine and Oxygen involving the (α,n) reaction in dry UO2F2 compounds and the nSA for spontaneous fission for isotopes of Uranium [4], [5].

Isotope	**F in UO_2F_2 (n/s/g) ±2% RSD**	**O in UO_2F_2 (n/s/g) ±3% RSD**	**Spontaneous Fission (n/s/g)**
^{234}U	1.97E+02	2.26E+00	6.71E-03 ± 10%
^{235}U	3.82E-02	5.27E-04	1.05E-05 ± 30%
^{238}U	3.93E-03	6.05E-05	1.334E-02 ± 1.7%

Table 2 Neutron Specific Activity (nSA) for dry and wet UO2F2 and for solid UF6 [5].

Isotope	**"Dry" UO_2F_2 (n/s/g)**	**"Wet" UO_2F_2 (n/s/g)**	**Solid UF_6 (n/s/g)**
^{234}U	1.99E+02 ± 2.01%	1.73E+02 ± 5.38%	†5.03E+02 ± 2.60%
^{235}U	3.87E-02 ± 2.07%	2.79E-02 ± 7.17%	1.22E-01 ± 7.38%
^{238}U	3.99E-03 ± 2.01%	3.69E-03 ± 5.42%	1.43E-02 ± 14.0%

† UF_6 U-234 nSA obtained from [6].

A serious challenge to measuring the neutrons generated from UO2F2 is subtracting the background neutrons generated by cosmic ray induced nuclear spallation [7], [8]. In addition, the variance of the Cosmic-Ray Spallation (CRS) rate during the day and during a measurement period can be difficult to account for [9]. Background neutrons arise from cosmic ray interactions with the atmospheric layers above, with the ground below and with the structural components from building materials in the immediate vicinity. In addition, the large metallic mass of the object (plant equipment) itself, will significantly contribute to the neutron background.

The remaining content of this paper addresses the principles of the phased design and implementation of the final design which includes the methods and analysis processes. In addition, we describe the successful Verification and Validation (V&V) of the newly constructed Large Item Neutron Assay System (LINAS) chamber at the PGDP site.

DESIGN

The design of the LINAS was broken into several phases involving a design group consisting of subject matter experts, physicists, civil and mechanical engineers. At each phase, a thorough design review was conducted and any changes applied to the next design phase. The main objectives of the design were to meet, or beat, disposition performance objectives, abide to a reasonable schedule within the budget, and reuse any existing equipment and hardware that may be available such as HDPE shielding and He-3 for neutron detection, specifically, there were 124 two atmospheres (atm) He-3 pressurized tubes available from a prior system [10].

Data Quality Objectives

The design of any nuclear waste characterization system reflects the disposition requirements set by the waste generators as well as federal, state and local regulations. The primary disposition and performance objectives, *i.e.*, Data Quality Objectives (DQO's), were defined during the first phase of the design and consist of the following:

- Accommodate objects as large as the '000' converter and objects as small as 24" diameter pipe as well as 20' intermodal and Sealand waste containers.
    - The objects are transported via large carts with support cradles, using a tow motor, which have much metallic weight. The carts and cradles are included in the measurement process but the tow motor is not since it is removed from the chamber prior to measurement.
- U-235 Minimal Detectable Activity (MDA) of 25 grams or less for any given object, *i.e.*, plant equipment, and from any cascade at the PGDP site.
    - Minimize CSTEEL materials throughout to minimize CRS.
- Total Measurement Uncertainty (TMU) of 35% or less, 1-sigma, for any given object.

    - Uniform detection efficiency fields.
- High Throughput
    - Capable of 10 or more objects per day.
    - Target measurement time of 30 minutes.
    - Tow motor entrance and exit positions with two sliding doors for each position.
- Service period of at least 50 years

Detectors

The two inch diameter, 40" active length and two atm (202.65 kPa) pressurized He-3 detectors (124 count) from the prior system were originally housed in the typical Decommissioning In-Situ Plutonium Inventory Monitor (DISPIM) [11] HDPE rectangular detector packages. The detectors/DISPIM packages were shipped to Mirion Technologies for inspection. The detector model and serial numbers were provided to the manufacturer, Reuter-Stokes, and the appropriate tube drawings were supplied and dimensions modeled in the MCNP V6.2 [13] application. Each and every one of the 124 He-3 tubes passed quality control inspection. The He-3 detectors were then bench tested for initial performance within the DISPIM packages and then removed from the DISPIM packages.

He-3 Distribution

Prior systems [10], [13] utilized a rectangular design for the layout of the He-3 detectors mostly due to the fact that the waste containers were rectangular. A rectangular design creates "corners" which can create non-uniform efficiency fields and limits the size and shape of the objects based on TMU and MDA goals. The basic cylindrical design has no such issues since the efficiency field is fairly uniform within the volume defined by the cylinder as long as the object is reasonably centered, *i.e.*, within a few feet, near the axial center of the cylindrical arrangement. In addition, much of the plant equipment at the PGDP site is cylindrical in nature so for these reasons a base cylindrical arrangement for the He-3 detector distribution was selected.

Given the basic cylindrical layout approach, the He-3 detectors and HDPE slab packages were redesigned which included a strategy to consume as many of the original detectors whilst optimizing sensitivity around the large metallic objects, *i.e.*, plant equipment. The optimal design yielded a three detector ring arrangement with several detector slab packages per ring, effectively producing a cylindrical geometry. To increase sensitivity, detector slabs were added to both ends of the cylindrical geometry which also reflected a design goal that there be four sliding doors. A further sensitivity study result was to limit the ring detector slab packages to five, per ring, with six He-3 tubes per ring slab package . The remainder of the He-3 tubes were distributed through four detector slab packages at the cylindrical ends with eight He-3 tubes per slab package. Overall, there were 30 He-3 tubes per ring, 90 ring positioned He-3 tubes in total, and 32 He-3 tubes at the cylindrical ends. *i.e.*, entrance and exit doors. This optimal strategy consumed 122 of the 124 tubes leaving two He-3 tubes as spares. There are 19 detector slabs in total; 15 ring detector slabs and four door detector slabs.

HDPE Detector Slab

The design of the LINAS detector slabs involved the optimal positioning of the two inch diameter He-3 tubes withing the HDPE slab with the basic design shown in Fig. 2. The single slab design that supports both the ring and door detectors accommodates up to eight, two inch, He-3 tubes with the two end tube slots optionally plugged. This facilitates flexibility with a single slab design for both six and 8 He-3 tube packages. In addition, the two inch diameter HDPE rods can be removed for future He-3 expansion for the six He-3 tube slabs designated for the rings. Surrounding the LINAS detector slab, on five of the six sides, is a two inch thick borated (5%) HDBPE shield. The purpose of the HDBPE is to shield against any thermal/epithermal neutrons which might be of CRS origin produced from cosmic ray interactions within the surrounding structural components. The detector slab electronics include three amplifiers per slab so there are 57 separate neutron signal inputs.

Chamber

The purpose of the LINAS chamber is to support the detector ring structure, support the doors and door detectors, provide the necessary cosmic ray shielding and accommodate the largest of the plant equipment which is the '000' converter at 13.5' diameter and 24' in length. In addition, the chamber structure must facilitate moving plant equipment in and out of the chamber and provide functionality for centering and staging the plant equipment for assay.

The basic cylindrical/ring arrangement was modeled using MCNP V6.2 [14] for optimal efficiency considering the range of objects, *i.e.*, plant equipment. The extent, *i.e.*, geometry, of the object and the object weight is considered in the models. The geometry of the object is defined by the spatial distribution relative to the detectors. The massive CSTEEL weight of the object will moderate neutrons altering the system detection efficiency. Adding the MCNP models for the 15 ring oriented detectors and the four door detectors, the optimal geometry for all plant equipment determined the detector ring spacing for the three rings. The detector package layout on the ring structure was, however, not optimal as it was not possible for detectors to be under the object due to the cart position. Breaking symmetry and omitting the bottom ring position, the semi-optimal ring detector position design was to uniformly distribute the slabs relative to a top-center ring detector with the lower detector slabs near the cart height. The four door detectors were strategically placed flush with the inside of the sliding doors with an optimal elevation.

The structure that defines the LINAS chamber involves a three foot thick concrete (2.32 g/cc) ceiling with two foot thick concrete walls which act as shields from cosmic-ray interactions. The basic inner dimension of the chamber is 32' long, 22' high and 22' wide. The base concrete foundation is 36" with an additional 10" of concrete floor providing a full 46" of support and shielding from cosmic-ray interactions from the soil below. The final LINAS chamber design is shown in Fig. 3 where a LINAS chamber top view and front (door) view are provided. The optimal design yields the ring diameter of 15', detector face to face, which easily accommodates the '000' converter. The rings are separated by 75" and the detector slabs within the ring are separated by 60^{o}. The door detectors are 32' face to face (entrance to exit).

The z-plane cross section of the LINAS chamber is shown in Fig. 4 depicting the layout of the concrete walls, ceiling, floor and detector rings. The concrete is strengthened using ASTM A615 Grade 60 Steel reinforcing bar (rebar) with the following distribution:

- Two layers steel rebar per concrete slab (two wall slabs , one roof slab and one floor slab).
- Each layer of steel rebar is 2.5 inches within the two surfaces of the concrete slabs.
- Five tons of steel rebar in the roof slab (2.5 tons per layer).
- 4.3 tons of steel rebar per wall slab (2.2 tons per layer).
- 8.2 tons of steel rebar in the LINAS floor slab (4.1 tons per layer).

This concrete reinforcement information was included within the MCNP models.

The detector ring structures, shown in and Fig. 4 and Fig. 5, are made entirely of Aluminum with only CSTEEL materials from ten 8"x18" I-beam support inserts and two lengthwise 8"x31' I-beam supports. The detector ring horizontal and vertical supports are made of special Aluminum I-beams and are fully plumbed and stabilized so as to minimize vibrations which could potentially cause detector microphonics. The total weight of each Aluminum detector ring, including detector supports, is approximately 2,100 lbs. All the metal utilized for the detector rings and support was included in the MCNP models.

The chamber sliding doors are 9" thick consisting of 1"x 4'x8' sheets of HDPE supported by Aluminum framing. The doors overlap the chamber shield at the top and sides and are a few inches below flush with the concrete floor.

There are four doors, two on each side, which move in independent opposing motions so as to facilitate a full opening for both the entrance and exit sides which supports loading of plant equipment via the cart and tow motor. There are door bottom rollers which move along a track cut into the concrete floor with motors and pulleys to facilitate door opening/closing. Limit switches guarantee that the doors are fully-closed or fully-open. Each of the four doors has an 8-tube detector slab mounted such that the bottom of the slab is in elevation 94" from the concrete floor and are edge-to-edge separated by 36" when the doors are fully closed. The doors are ship lapped by several inches so as to optimize the shielding capability of the doors when closed.

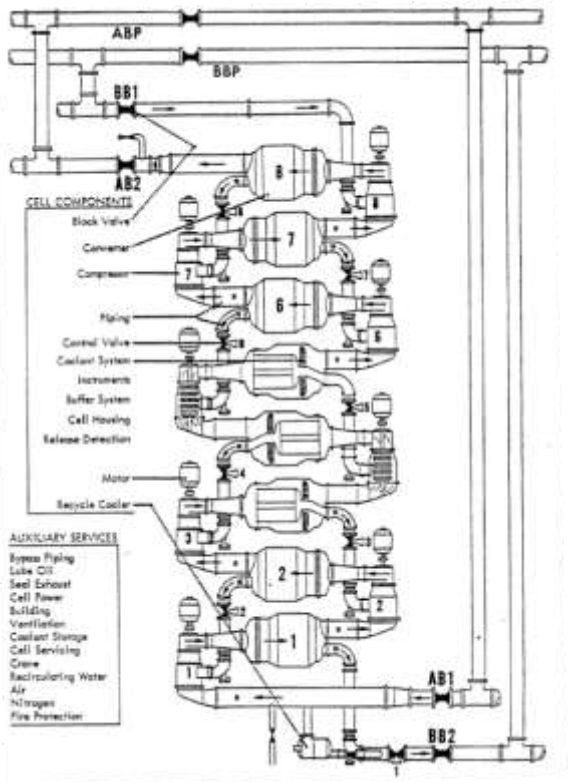

Fig. 1 Typical GDP cell arrangement showing the plant equipment which potentially contains holdup (reproduced from [6]).

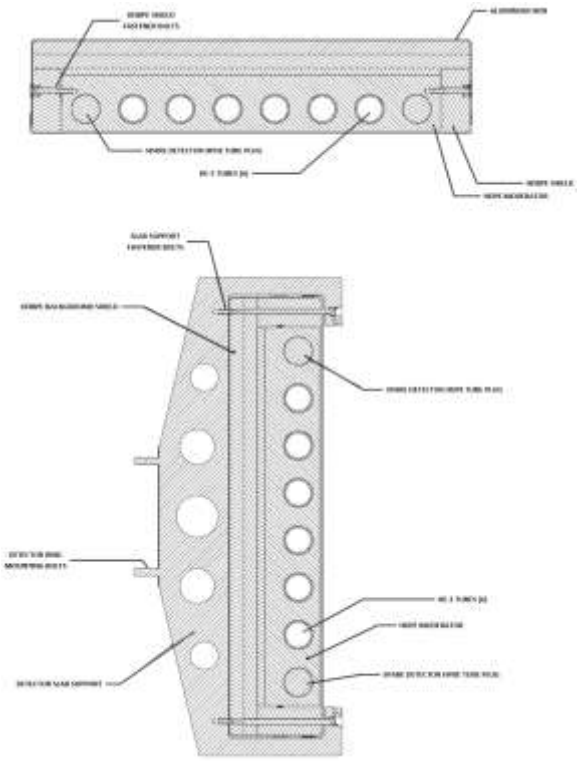

Fig. 2 Two and three-dimensional images of the LINAS detectors. The two dimensional images (left) show the six-tube arrangement with the two HDPE plugs inserted for the six detector arrangement. The three dimensional image (right) shows the ring support brackets utilized for both the six and eight detector LINAS slabs.

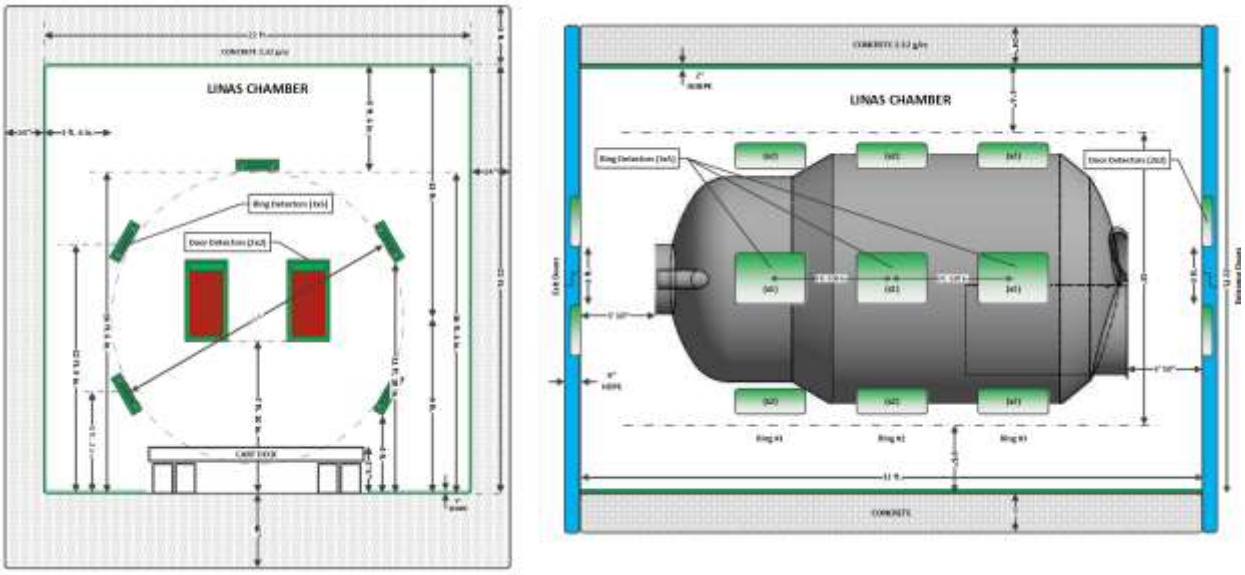

Fig. 3 Front view (left) and top view (right) of the LINAS chamber. The top view incudes the 000 bulged converter which is the maximum diameter object (plant equipment).

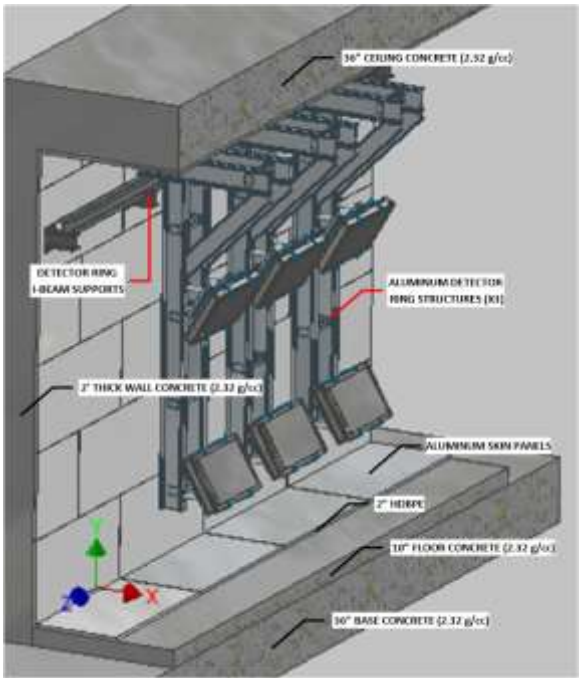

Fig. 4 Cross-section (z-plane) of the LINAS chamber (doors not shown).

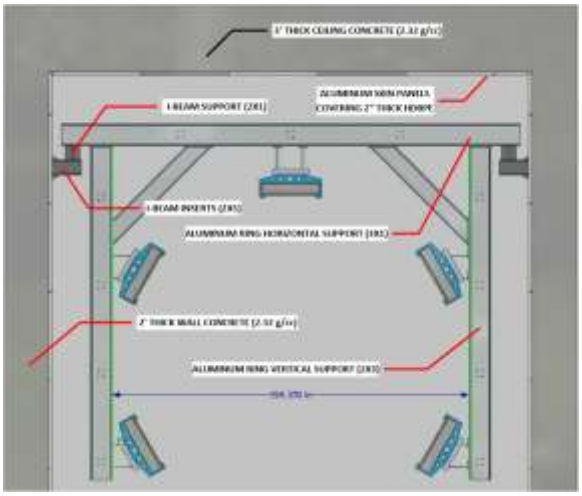

Fig. 5 Detector ring structure and support within the LINAS chamber.

Data Acquisition Principles

The Data Acquisition System (DAS) involves two sets of electronics; a high-performance scaler summing module and a high performance coincidence shift register module. The scaler summing module is the Mirion JSB-96 scaler analyzer which contains a high-speed Field Programmable Gate Array (FPGA) to facilitate de-randomizations with a pulse pair resolution of 20 ns.

This de-randomization process ensures that deadtime is kept to a minimum and providing a premium quality summed pulse stream to the coincidence analyzer. The JSB-96 scaler module also records and displays the 57 preamplifier output channels. The coincidence analyzer is the high-performance JSR-15R (rack mounted) shift register analyzer with a time resolution matching that of the JSB-96 output. The JSR-15R produces 512 multiplicity channels for both the *reals* and *reals + accidentals* gates. The high-quality multiplicity histograms are utilized to veto massive cosmic-ray events which may lead to high-ordered neutron multiplicities from spallation resulting in an elevated singles rate and associated variance. The neutron multiplicity histograms are acquired in 30 second cycles and any cycle that detects a high multiplicity event might be rejected based on certain criteria during acquisition and post-acquisition, *e.g.*, data reanalysis. Based on site experience and CRS models for the elevation/geomagnetic rigidity [7], [9], [15] of the Paducah site, the frequency of such massive neutron producing spallation events has periods much longer than that of 30 second cycles. The expectation is that 1/10 to 1/20 thirty second cycles might be rejected where the frequency of rejection depends on how much CSTEEL mass is in the LINAS chamber. The overall effect of the cycle vetoing is to reduce the variance in the singles and coincidence rates and produce a true singles rates that best represents the detected neutrons emitting from UO2F2 holdup.

IMPLEMENTATION AND METHODS

Construction

Concrete was poured using a specialized method involving entrained air with strict slump, temperature, air and strength tests assessed prior to the concrete pour. The purpose was to ensure that any voids and honeycombing effects were minimized yielding a uniform density of 2.32 g/cc. The 8”x18” I-beam CSTEEL support anchors were inserted during the concrete pour for maximum support strength. The Aluminum detector rings and detector supports were fabricated offsite and shipped while the concrete was curing. Once the concrete was cured, the 8”x18” I-beam supports were fastened to the support anchors and the two lengthwise 8”x31’ I-beams were fasted to the supports. The three Aluminum I-beam ring structures were attached along the chamber length defining the three detector rings. The detector supports for the overhead detector and four side detector supports, were attached, per ring, as shown in Fig. 6

The Aluminum frames for the four doors were fabricated offsite and installed at the LINAS chamber entrance and exit sides. The 1”x4’x8’ sheets of HDPE were then attached to the Aluminum frames using a special fastening technique. The inner few layers of the 9” thick HDPE doors were excavated to accommodate a flush mounting the four door detectors.

All detector signal, high- and low-voltage, cables were routed to a separate, fully enclosed climate controlled box, housing the JSB-96 mounted to the exterior of the LINAS chamber ensuring along the route that no excessive force or pinch points were engaged, especially when the doors are opened and closed The summed signal from the JSB-96 is sent to the JSR-15R in a separate climate controlled control room, just a few feet away from the chamber. The LINAS chamber and control room are also enclosed by a large climate controlled prefabricated building with both entrance and exit vertical bay doors so as to accommodate pulling the plant equipment through the LINAS chamber.

Detectors and Data Acquisition

The detectors, associated cabling and DAS electronics, were completely fabricated and bench tested at the factory and then delivered to the PGDP site well before the LINAS chamber was completed. A mock LINAS system was constructed in a separate building with the detectors arranged in a similar fashion, but much smaller than the LINAS ring design, and with no concrete shielding. The purpose of this mock LINAS testing was to verify the operations of the cabling and electronics, post shipment. and to sample some of the detector performance before final installation. Once the detector rings were installed within the LINAS chamber, the mock LINAS was disassembled. Having been fully tested, the DAS electronics and associated cabling were then installed within the LINAS chamber along with the detector slabs.

Carts/Cradles

Only the cradles for the standard cart were built for the initial production implementation of the LINAS. These standard cart/cradle enragements support all plant equipment with the exception of the '000' compressor and '000' converter as indicated in Table 3. The '000' compressor and '000' converter have existing designated carts with cradles.

Fig. 6 Installation of the three detector rings within the LINAS chamber.

Table 3 Carts and cradles designed for the supporting the plant equipment.

Cradles	Weight (lbs)
UC (Universal Cradle)	1,531
UC+Pipe Chocks	1,633
00 Converter	1,102
00 Compressor	473
000 Bundle C/D	1,053
Intermodal/Sealand	80
Carts	**Weight (lbs)**
Standard	12,980
WM Cart (surrogate)	3,000

Methods and Analysis

The primary method is to convert a measured neutron signal, for a given sample, to a filtered net singles rate, *i.e.*, properly background subtracted. The net singles rate is proportional to the U-235 mass in grams given the nSA of the Uranium compound (UO2F2, UF6), the Uranium isotopics, enrichment and the neutron detection efficiency for the sample geometry and CSTEEL mass. The nSA with the isotopic ratios is used to compute the neutron emission sum from the (α, n) and spontaneous fission contributions. The sample detection efficiency is computed from appropriate models including a voxelization approach. The U-235 mass calibration parameter of the sample is a product of the nSA and detection efficiency divided by the enrichment. Simply dividing the net singles rate by the calibration parameter produces the U-235 mass in grams.

The biggest challenge is the neutron rate within the chamber which involves sources of neutrons not involving the Special Nuclear Material (SNM). CRS observed within the Empty Chamber (EC) and CRS from the metallic mass of the plant equipment itself must be subtracted. Additionally challenging, is that the CRS rates can fluctuate during the day and will vary, considerably, over extended periods including weeks, months and years. The daily/weekly/monthly fluctuations are mostly due to differences in barometric pressure and, to a lesser extent, diurnal solar fluctuations. The yearly fluctuations are due to solar seasonal events; multiple-year fluctuations are due to galactic events such as the Forbush decrease event [7]. The CRS background and associated fluctuations must be fully accounted for, providing an improved accuracy as well as the lowest possible TMU and MDA.

An investigation and measurement campaign covering a three-month period involved observing the CRS rates within the LINAS chamber for the EC case and with various excess CSTEEL mass loadings up to 82K lbs as shown in Fig. 7. Various counting times ranging from 300 seconds to 24 hours were utilized.

The data points depicted in Fig. 7 show the singles neutron count rate for the EC, void of any excess CSTEEL (EC + 0), and then for excess CSTEEL loadings consisting of EC + 26K, EC + 36K , EC + 58K and EC + 82K lbs. The trend (x-axis) is barometric pressure (mbars) where a highly correlated trend is observed. The dash-dotted lines shown in Fig. 7 are the equivalent U-235 mass if the CRS rates were not removed. In the case for the EC + 82K lbs CSTEEL, the U-235 mass ranges from 278 g to 427 g U-235 for 4.96% enrichment and 71 to 109 g U-235 for DU (0.2%) over the barometric pressure range of 1022 to 960 mbars. When only the EC + 0 is considered, the U-235 equivalent ranges from 157 g to 239 g U-235 for 4.96% enrichment and 40 to 61 g U-235 for DU (0.2%) also over the barometric pressure range 1022 to 960 mbars. To have quality measurement accuracies that accommodate the DQO's stated in the introduction section, the CRS and the variance in the CRS, for the EC and EC plus excess CSTEEL must be well quantified for each measurement and subtracted. This CRS quantification amounts to a parameterization of the EC (EC + 0) and excess chamber CSTEEL (EC + CSTEEL) as a function of barometric pressure. Regarding counting time, there was no benefit in counting longer than 3600 seconds as the counting statistics did not improve. In addition, there are variances due to pressure fluctuations that come into play for counting times longer than 3600 seconds. It was also determined that the absolute minimum count time is 600 seconds due to counting statistics.

Using the inspiration from the measurement campaign and the work from [7] and [8], a method was developed where the CRS observed neutron detection rate, $R(P)$, for both the EC and excess CSTEEL (EC + CSTEEL) were parameterized as a function of barometric pressure of the form,

$$R(P) = R_o \cdot e^{-\beta \cdot (P - P_o)} \qquad \text{Eq. 1}$$

where R_o is an arbitrary reference rate at the reference barometric pressure, P_o. The β parameter is a free fit to the measured data points shown in Fig. 7. The EC and EC + CSTEEL were fitted separately so two β parameters were determined,

$$\beta_{EC} = 6.753 \times 10^{-3} \pm 8.554 \times 10^{-5} \qquad \text{Eq. 2}$$

and,

$$\beta_{EC+CSTEEL} = 6.942 \times 10^{-3} \pm 2.105 \times 10^{-4} \qquad \text{Eq. 3}$$

The CRS rate versus chamber excess CSTEEL calibration was computed at P_o=1000 mbars from the observed rates shown in Fig. 7 using Eq. 1 and Eq. 3 where the reference rate, R_o is computed as the average rate over the measured barometric pressure range. The fitted result is shown in Fig. 8 where a linear fit is determined,

$$slope = \boldsymbol{m} = 8.688 \times 10^{-5} \pm 1.876 \times 10^{-6}\ (cps/lb)\ @\ P = 1000\ mbars \qquad \text{Eq. 4}$$

$$intercept = \boldsymbol{b} = 9.05 \pm 0.02\ (cps)\ @\ P = 1000\ mbars \qquad \text{Eq. 5}$$

The intercept, $\boldsymbol{b}$, is simply the EC + 0 rate at the barometric pressure of P=1000 mbars.

The method involves discarding the intercept, $\boldsymbol{b}$, since the daily, seasonal and galactical fluctuations must be accounted for. Thus, the method requires that the EC, *i.e.*, EC + 0, background be measured each day, within a 24 hour period, with the barometric pressure tagged ($P_o = P_B$). The EC rates are then converted, utilizing Eq. 1 and Eq. 2, to the EC rate equivalent for the barometric pressure, P, at the measurement time for the plant equipment. The EC + CSTEEL rate contribution utilizes the slope parameter (Eq. 4) and the rate converted from $P_o = 1000$ mbars to the barometric pressure , P. This facilitates the computation of the net rate, R_{NET},

$$R_{NET} = R_{SAMP} - \boldsymbol{m} \cdot GW \cdot e^{-\beta_{EC+CSTEEL} \cdot (P - 1000)} - R_{EC} \cdot e^{-\beta_{EC} \cdot (P - P_B)} \qquad \text{Eq. 6}$$

Where R_{SAMP} is the measured sample rate, $\boldsymbol{m}$ is the slope parameter (Eq. 4), *GW* is the gross weight in lbs, R_{EC} is the EC + 0 rate measured within a 24 hour period of the sample measurement, GW is the sample gross weigh in lbs and includes the weight of the cart and cradles. The range of EC and sample counting times was determined to be no less than 600 seconds but no more than 3600 seconds to accommodate the DQO's. The target production measurement time is 1800 seconds and the barometric pressure is recorded for every measurement and consumed by the rates analysis, specifically, Eq. 6.

The U-235 mass calibration involves the assigned neutron detection efficiency, enrichment and Uranium neutron specific activity, SA_U,

$$SA_U = \sum_i \sum_j nSA_{ij} \cdot wf_j \qquad \text{Eq. 7}$$

where,

nSA_{ij} = Neutron specific activities from Table 1 and Table 2.

wf_j= Weight fraction for each contributing isotope of uranium ($j \rightarrow 234, 235\ and\ 238$).

The weight fractions are not always known for each sample but the enrichment and the U-235:U-234 weight percent ratio are typically known for the cascade from which the plant equipment was extracted. Optionally, sampling and laboratory analysis may be utilized. The weight fraction, in either case, is calculated as follows:

$$wf_{234} = \frac{wf_{235}}{wf_{ratio}} \qquad \text{Eq. 8}$$

Where wf_{ratio} is the known U-235:U-234 weight fraction ratio for the representative cascade.

The U-235 mass calibration parameter, a_{obj}, for the object (plant equipment) is computed,

$$a_{obj} = \frac{SA_U \cdot \epsilon_{obj}}{(E/100)} \qquad \text{Eq. 9}$$

where the enrichment, E, is defined by the cascade and the efficiency for the object, ϵ_{obj}, is determined by modeling the geometry and the CSTEEL mass (weight) of the object.

The U-235 mass is then simply the object net rate divided by the U-235 calibration parameter,

$$g^{235}U = \frac{R_{obj}}{a_{obj}} \qquad \text{Eq. 10}$$

where, $R_{obj} = R_{NET}$ as defined in Eq. 6.

TMU

The uncertainty in the net rate is determined by performing the standard error analysis on Eq. 6 where all sources of error are propagated and added in quadrature. The TMU is computed as a quadrature sum of several individual contributions expressed mathematically as,

$$TMU = \sqrt{\sigma_{ST}^2 + \sigma_E^2 + \sigma_{MODEL}^2 + \sigma_{SIG}^2 + \sigma_{BKGD}^2 + \sigma_{GEO}^2} \qquad \text{Eq. 11}$$

where,

σ_{ST} = uncertainty due to sample type considerations, i.e., variations in nSA, *e.g.*, "wet" vs. "dry", UO_2F_2 mixing with UF_6 as defined in Table 2.

σ_E = enrichment variations,

σ_{MODEL} = uncertainty in the efficiency attributable to modeling (MCNP/voxelization)

σ_{SIG} = uncertainty due to measurement counting statistics,

σ_{BKGD} = uncertainty due to variations in background,

σ_{GEO} = uncertainty in the efficiency attributable to geometrical variations

The above estimates for the primary contributors to the overall TMU are summarized in Table 4, along with an estimate for the overall TMU, obtained by summing the individual contributions in quadrature. The counting statistics and sample geometry dominate the %RSD for the example shown in Table 4. The %RSD counting statistics are generally much smaller as the counting time for the sample was only 900 seconds and the U-235 mass was only 5.37 grams of U-235 (DU) and near the computed MDA of 2.6 g U-235. The sample geometry %RSD includes variations in the CSTEEL spatial distribution of the object (sample) within the LINAS chamber, CSTEEL density effects within the sample and source (holdup) non-uniformity within the object.

Table 4 TMU budget for a very low U-bearing mass item with a gross weight of 21K lbs.

TMU Contributor	% RSD
Sample Type & Enrichment	7
Counting Statistics[A]	15
Background Variation Correction Factor	1
Modeling	7
Sample Geometry	14
Estimated TMU:	**23**

[A] The % RSD contribution from counting statistics represents an example value drawn from the V&V measurements corresponding to equipment with a low mass (5.37 g U-235) of depleted uranium (DU) and a counting time of 900 seconds.

Limit of Detection

The U-235 limit of detection, L_d, in cps, is computed as,

$$L_d = \frac{k^2 + 2 \cdot k \cdot \left(\frac{t_s}{t_o} \cdot \left(\left(R_{B_P} + R_{M_P} \right) \cdot t_s + \sigma^2_{R_{B_P}} \cdot ({t_s}^2 + {t_o}^2) + \sigma^2_{R_{M_P}} \cdot {t_s}^2 + R_{B_P} \cdot t_o \right) \right)^{1/2}}{t_S} \quad \text{Eq. 12}$$

where,

$R_{B_P} = R_{EC} \cdot e^{-\beta_{EC} \cdot (P - P_B)}$ extracted from Eq. 6

$\sigma^2_{R_{B_P}}$ is the computed variance in R_{B_P}.

$R_{M_P} = \boldsymbol{m} \cdot GW \cdot e^{-\beta_{CSTEEL} \cdot (P - 1000)}$ extracted from .Eq. 6

$\sigma^2_{R_{M_P}}$ is the computed variance in R_{M_P}.

t_s is the sample (plant equipment) measurement time in seconds.

t_o is the background (EC) measurement time in seconds.

k is the confidence interval (k=1.645 for a 5% false positive rate).

The U-235 MDA, in grams, is defined as,

$$MDA = \frac{L_d}{a_{obj}} \quad \text{Eq. 13}$$

Where a_{obj} is the sample U-235 calibration parameter extracted from Eq. 9. The MDA for several measurements involving a '00' converter surrogate (GW=44,000 lbs including cart and cradles) is shown in Fig. 9.

The measurements include various WRM U-235 mass loadings (27.9 to 735 g U-235), count times (t_s = 600 to 3600 seconds; t_o=1800 seconds) and enrichments (E = 0.2%, 0.7%, and 4.96%). The L_d ranges from 0.44 cps to 0.73 cps and the MDA ranges from 2.4 grams to 14.9 grams U-235 which is much in line of the stated DQO's.

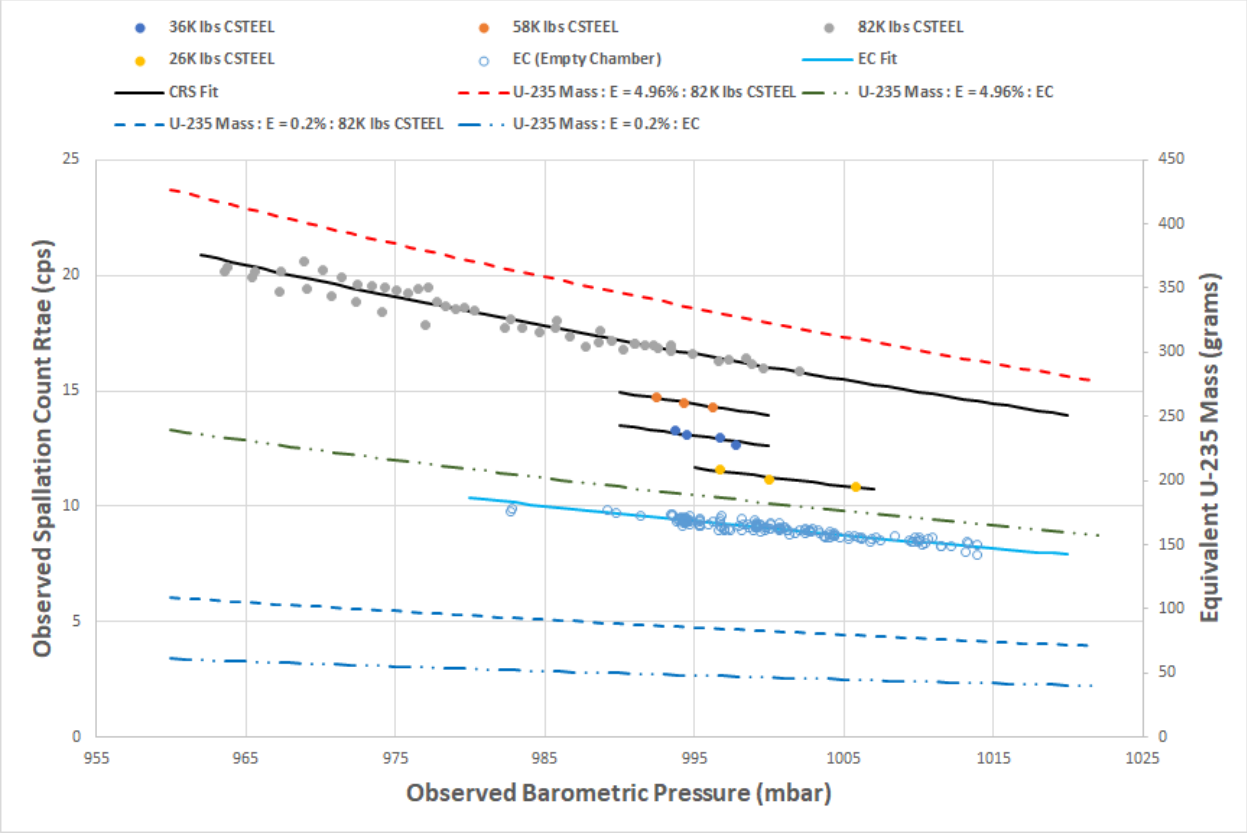

Fig. 7 Observed CSR rates for the EC and additional CSTEEL mass loadings showing the U-235 mass equivalence for DU (0.2%) and enriched U (4.96%). The uncertainty in the measured rates data points are less than the size of the markers with the exception of the EC + 82K lbs where the uncertainty is 2x to 3x the marker size for barometric pressure less than 978 mbar.

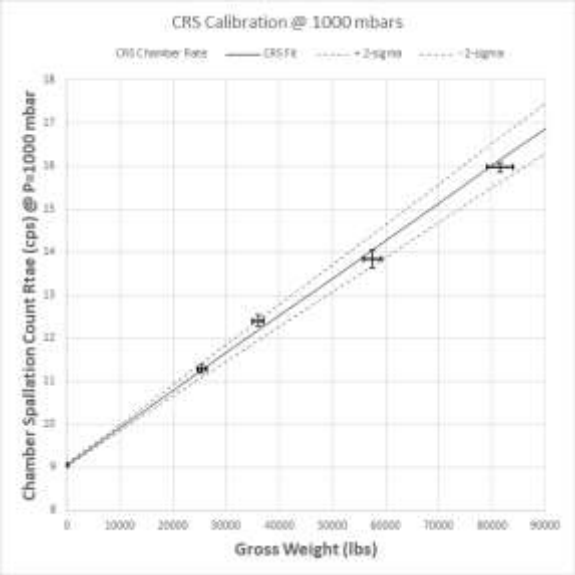

Fig. 8 The measured CRS rate as a function of additional CSTEEL mass converted to a barometric pressure of 1000 mbars.

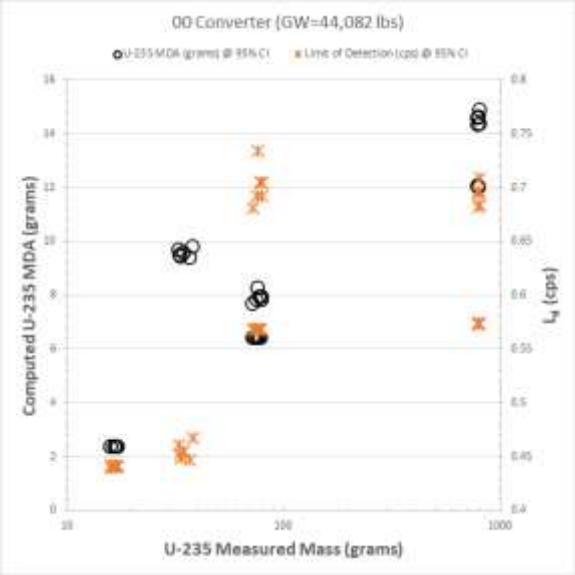

Fig. 9 MDA and L_d for the '00' converter (*GW*=44K lbs) involving various WRM U-235 mass loadings, sample (counting) times and enrichments.

VERIFICATION AND VALIDATION

The Verification and Validation (V&V) plan included several objects covering a dynamic range of object shapes and CSTEEL weights. The selected objects are called surrogates since they represent the plant equipment and have provisions for placing WRM's in strategic positions including Volume Weighted Average (VWA) and non-VWA distributions. The surrogates utilized for the LINAS V&V are listed in Table 5 where the surrogate length width, height and weight, not including the cart/cradle weight, are shown. Also depicted in Table 5, are the VWA neutron detection efficiencies which were generated using a voxelization approach employing a series of MCNP models as a basis. These VWA efficiencies most closely represent the shape, weight and cart/cradle positioning of the surrogate within the LINAS chamber.

The WRM's included various enrichments such as Depleted Uranium (DU) at 0.2%, "normal" enrichment at 0.7%, "low" enrichment at 1.0% and the plant limit "high" enrichment at 4.96%, configured in various formats as depicted in Table 6. Each WRM utilized for the V&V has an associated certificate declaring the U-234, U-235 and U-238 weight percent or the enrichment and the U-235:U-234 weight percent ratio. The numerous available WRM's are relatively small in size with special formats which facilitates placing many WRM's within any of the surrogates. The highest mass loading configuration was 735 grams U235 and the lowest configuration was 5.37 grams of U-235.

The main emphasis of the V&V was to arrange the WRM's in VWA configurations with a secondary goal to stress test the TMU and limit of detection (MDA) in relation to the DQO's. The VWA configurations were simulated by strategically placing the WRM's throughout the surrogate which best represents the modelled efficiencies. The TMU tests are primarily for simulating deposits and were accomplished by placing the WRM's in non-VWA positions such as grouped at one end, or side, of the surrogate and/or at the very bottom or top of the surrogate. To achieve the limit of detection tests, various very low U-235 mass WRM configurations were placed within the surrogate. The target recovery, for six replicates, is ± 30% with a replicate percent Relative Standard Deviation (%RSD) limit of ± 14%. Given the method range of 600 seconds to 3600 seconds for a counting time, a variety of counting times were also selected as additional tests for the VWA, TMU and MDA configurations. The calibration parameter (Eq. 9) was computed for each configuration and utilized the "dry" nSA in Table 2.

The V&V results for the entire campaign are shown in Fig. 10 where all replicate measurements satisfied the target recoveries. The average weighted recovery was 92.7% (horizontal dashed line) and the average %RSD was 4.1%. The data points near the high- and low-end of the recoveries are the high- and low-bias TMU configurations simulating potential deposits expected when the LINAS is in production. The measurements with large error bars are a direct result of detection limit and MDA tests involving low-mass WRM configurations and/or shorter counting times.

Table 5 Physical properties and parameters utilized for the plant equipment surrogates utilized for the calibration confirmation.

Surrogate	Length (in)	Width (in)	Height (in)†	Weight (lbs)	Eff (%)
00 Converter Surrogate	209	106	103	27,420	2.25
30" G-17 Valve Surrogate	44.5	50	115	2,930	2.36
54" Square-to-Round Surrogate	61	54	54	1,094	2.36
30 " diameter x 19 ft. Pipe Surrogate	228	30	30	1,887	2.18
Windmill (WM) Surrogate	24	132	0	640	2.28
ST-90 Surrogate/7 Drums/Metals	86	48	48	4,136	2.36
Bundle Surrogate directly on Cart	216	132	117	11,182	2.25

† If height is zero then the object is considered to be cylindrical in shape and the width is the diameter.

Table 6 Working reference materials utilized for the calibration/confirmation effort.

ID	Format	Enrichment		g U-235 per WRM
		Description	E (%)	
1x9NORM	1"x9" Tubes	Normal	0.711	1.33
1x9ENR	1"x9" Tubes	Enriched	4.973	9.19
1x9DU	1"x9" Tubes	Depleted	0.231	0.447
3x5NORM	3"x5" Cylinders	Normal	0.711	13.5
PSIENR1	UF6 psi tubes	Enriched 4.9	4.908	1.29
PSIENR2	UF6 psi tubes	Enriched 1.0	1.012	0.271

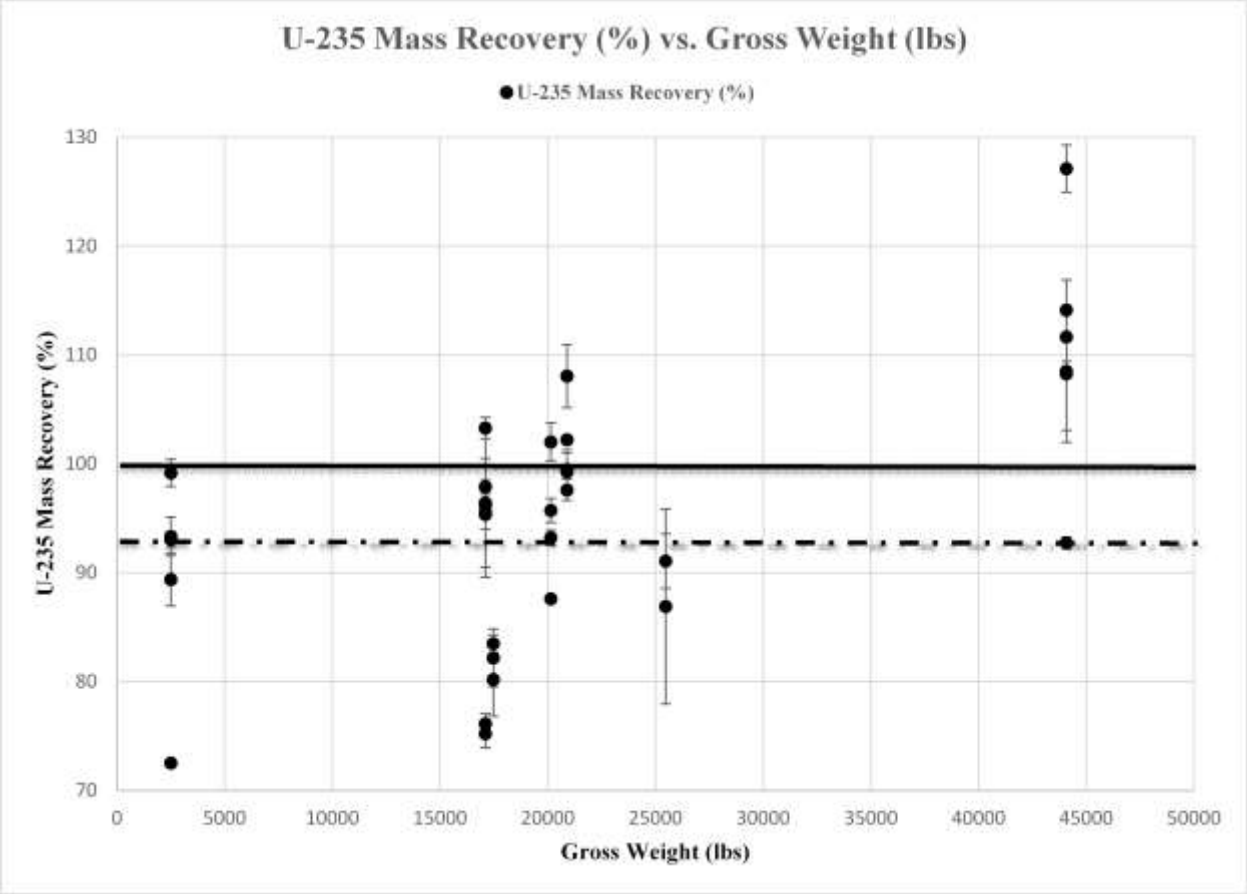

Fig. 10 Recoveries for the LINAS V&V. The error bars are the standard deviation of the replicates.

CONCLUSION

We have designed, implemented and validated the Large Item Neutron Assay System (LINAS) currently in operation at the Paducah Gaseous Diffusion Plant (PGDP) in Western Kentucky. The LINAS consists of 19 HDPE neutron slab detectors consisting of122 pressurized He-3 tubes at two atm, two inches in diameter and 40" active length in a ring arrangement within a thick concrete shielded chamber. The Data Acquisition System (DAS) is located within an electronically attached external control room all surrounded by a climate controlled prefabricated building. The LINAS is capable of characterizing Uranium holdup within large scale metallic plant equipment, extracted from the cascades, containing passivation layers and UO2F2 deposits utilizing an analysis method involving the detection of (α,n) and spontaneous fission neutrons and a novel method for subtracting neutrons of cosmic ray induced spallation origin. The LINAS has been subjected to a thorough V&V program with a range of enrichment and U-235 mass loadings up to 735 g U-235. The LINAS supports plant equipment from all cascades at the PGDP site which includes an enrichment range from DU to the highest plant enrichment of 4.96%. The Minimum Detection Activity (MDA) is below 25 grams of U-235 for the largest plant equipment where a majority of the plant equipment has an MDA less than 15 grams of U-235. The Total Measurement Uncertainty (TMU) is below 25% for all plant equipment for the shortest counting time and for U-235 holdup near the MDA. The LINAS structural design and methods allow for high throughput where the sample measurement time can be as low as 600 seconds and the optimal sample counting time is 1800 seconds. The LINAS method only requires that an EC background be measured once in 24 hour period.

REFERENCES

[1] NRC, "Gaseous Diffusion Enrichment," [Online]. Available: https://www.nrc.gov/materials/fuel-cycle-fac/ur-enrichment.html#diffusion.

[2] R. L. Mayer, J. D. Litteral, K. D. Banks, J. B. Montgomery, B. M. Lanning and B. P. Lynch, "Neutron Specific Activity of Uranium Isotopes In UO2F2," in *Proceedings of the 49th Annual Meeting of the Institute of Nuclear Materials and Management (INMM)*, Nashville, TN, 2008.

[3] B. Morel, "Surface Reactivity of Uranium Hexafluoride (UF6)," Comptes rendus de l'Académie des Sciences, France, 2018.

[4] ASTM-C1807-15, *Standard Guide for NDA of SNM Holdup Using Passive Neutron Measurement Methods*, ASTM International, 2015.

[5] A. M. LaFleur, S. Croft, M. L. Richard, M. T. Swinhoe, D. R. Mayo and B. A. Sapp, "Traceable Determination of the Absolute Neutron Emission Yields of UO2F2 Working Reference Materials," in *2013 3rd International Conference on Advancements in Nuclear Instrumentation, Measurement Methods and their Applications (ANIMMA)*, Marseille, France, 2013.

[6] B. Montgomery, *Private Communications - Paducah Site nSA for wet/dry UO2F2 and solid UF6*, Paducah, KY: Outlook E-Mail, 2023.

[7] J. A. Kulisek, B. S. McDonald, L. E. Smith, M. A. Zalavadia and J. B. Webster, "Analysis of an Indirect Neutron Signature for Enhanced UF6 Cylinder Verification," *Nuclear Instruments and Methods in Physics Research*, vol. 846, 2017.

[8] B. Rossi, High Energy Physics, Prentice-Hall, Inc., 1952.

[9] K. Pushkin and M. Villani, "Shielding Materials for Low Radioactive Background Projects," in *WM2021 Conference*, Phoenix, Arizona, USA, 2021.

[10] A. Simpson and M. Clapham, "Methods for Reduction of the Minimal Detectable Activity in Neutron Assay of High Mass/High Z Objects," in *WM2014 Conference*, Phoenix, AZ, 2014.

[11] K. J. Eger, H. S. Smiley, J. W. Thiesing and K. E. Howe, "Summary Level System Description for the Uranium Neutron Counting System (UNCS) (BJC/OR-3126)," East Tennessee Technology Park (ETTP), Oak Ridge, TN, 2008.

[12] C. H. Orr, J. P. Ronaldson, S. Jones and G. Mottershead, "USE OF NOVEL NEUTRON COUNTING SYSTEMS TO SATISFY DIVERSE AND CHALLENGING MEASUREMENT NEEDS WITHIN THE DOE COMPLEX," in *WM'2000 Conference*, Tuscon, AZ, 2000.

[13] C. J. Werner, "MCNP User's Manual - Code Version 6.2," Los Alamos National Laboratory, Los Alamos, New Mexico, 2017.

[14] C. H. Orr, "ASSAY OF URANIUM CONTAMINATED WASTE IN INTERMODAL CONTAINERS BY PASSIVE NEUTRON MEASUREMENT AT THE OAK RIDGE 3 BUILDING D&D PROJECT," in *WM'01 Conference*, Tucson, AZ, 2001.

[15] NRC, "MODULE 2.0: GASEOUS DIFFUSION," [Online]. Available: https://www.nrc.gov/docs/ML1204/ML12045A050.pdf.

[16] W. N. Hess, Introduction to Space Science, Gordon and Breach Science Publishers, 1965.